

The Beam Thrust Cross Section for Drell-Yan at NNLL Order

Iain W. Stewart, Frank J. Tackmann, and Wouter J. Waalewijn

Center for Theoretical Physics, Massachusetts Institute of Technology, Cambridge, Massachusetts 02139, USA

At the LHC and Tevatron strong initial-state radiation (ISR) plays an important role. It can significantly affect the partonic luminosity available to the hard interaction or contaminate a signal with additional jets and soft radiation. An ideal process to study ISR is isolated Drell-Yan production, $pp \rightarrow X\ell^+\ell^-$ without central jets, where the jet veto is provided by the hadronic event shape beam thrust τ_B . Most hadron collider event shapes are designed to study central jets. In contrast, requiring $\tau_B \ll 1$ provides an inclusive veto of central jets and measures the spectrum of ISR. For $\tau_B \ll 1$ we carry out a resummation of $\alpha_s^m \ln^m \tau_B$ corrections at next-to-next-to-leading-logarithmic order. This is the first resummation at this order for a hadron-hadron collider event shape. Measurements of τ_B at the Tevatron and LHC can provide crucial tests of our understanding of ISR and of τ_B 's utility as a central jet veto.

Introduction. Event shapes play a vital role in the success of QCD measurements at e^+e^- colliders. This includes the measurements of $\alpha_s(m_Z)$, the QCD β function and color factors [1], and the tuning and testing of Monte Carlo event generators (see e.g. Refs. [2]). Event shapes for the more complicated environment at hadron colliders have been designed and studied in Refs. [3–6]. There is much anticipation that they can play a significant role at the Tevatron and LHC by improving our understanding of basic aspects of QCD in high-energy collisions such as the underlying event and initial- and final-state radiation, as well as nonperturbative effects. Here we focus on initial-state radiation (ISR). Strong ISR can significantly alter the partonic luminosity available for the hard interaction. Additional jets from ISR can also contaminate the jet signature for a specific signal. An ideal process to study ISR is isolated Drell-Yan production, $pp \rightarrow X\ell^+\ell^-$ with a veto on central jets. By vetoing hard central jets, the measurement becomes directly sensitive to how energetic and soft ISR contributes to the hadronic final state X .

Recently an inclusive hadron collider event shape τ_B was introduced, called “beam thrust” [6]. For $\tau_B \ll 1$, the hadronic final state consists of two back-to-back jets centered around the beam axis. The ISR causing these

jets occurs at measurable rapidities. In this limit τ_B provides similar information as thrust in $e^+e^- \rightarrow$ jets with the thrust axis fixed to the proton beam axis. For $\tau_B \sim 1$, the final state has energetic jets at central rapidities. Thus, requiring small τ_B provides an inclusive veto on central jets, while allowing ISR in the forward direction, as depicted in Fig. 1.

Experimentally, beam thrust is one of the simplest hadronic observables at a hadron collider. It requires no jet algorithms, is boost invariant along the beam axis, and can be directly compared to theory predictions that require no additional parton showering or hadronization from Monte Carlo programs. Beam thrust is defined as [6]

$$\tau_B = \frac{1}{Q} \sum_k |\vec{p}_{kT}| e^{-|\eta_k - Y|}, \quad (1)$$

where Q^2 and Y are the dilepton invariant mass and rapidity, respectively. The sum runs over all (pseudo)particles in the final state except the two signal leptons, where $|\vec{p}_{kT}|$ and η_k are the measured transverse momenta and rapidities with respect to the beam axis, and all particles are considered massless. The absolute value in the exponent in Eq. (1) effectively divides all particles into two hemispheres $\eta_k > Y$ and $\eta_k < Y$, where the former gives $|\vec{p}_{kT}| e^{-\eta_k} = E_k - p_k^z$ and the latter $|\vec{p}_{kT}| e^{\eta_k} = E_k + p_k^z$:

$$\tau_B = \frac{1}{Q} \left[e^Y \sum_{\eta_k > Y} (E_k - p_k^z) + e^{-Y} \sum_{\eta_k < Y} (E_k + p_k^z) \right]. \quad (2)$$

The dependence on Y explicitly takes into account the boost of the partonic center-of-mass frame, i.e. the fact that the collinear ISR in the direction of the boost is narrower, as depicted in Fig. 1. From Eqs. (1) and (2) we see that soft particles with energies $E_k \ll Q$ as well as energetic particles in the forward directions with $E_k - |p_k^z| \ll Q$ contribute only small amounts to τ_B . In particular, unmeasured particles beyond the rapidity reach of the detector are exponentially suppressed,

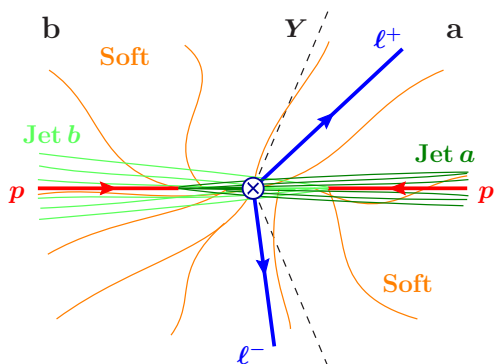


FIG. 1: Isolated Drell-Yan production with a veto on central jets.

$|\vec{p}_{kT}|e^{-|\eta_k|} \approx 2E_k e^{-2|\eta_k|}$, and give negligible contributions to τ_B . On the other hand, energetic particles in the central region with $E_k \pm p_k^z \sim E_k \sim Q$ give an $\mathcal{O}(1)$ contribution to τ_B . Hence, a cut $\tau_B \leq \tau_B^{\text{cut}} \ll 1$ vetoes central energetic jets without requiring a jet algorithm.

Beam thrust is also theoretically clean. It is infrared safe, and an all-orders factorization theorem exists for the cross section at small τ_B [6]. This allows for a higher-order summation of large logarithms, $\alpha_s^n \ln^m \tau_B$, and the calculation of perturbative and estimation of nonperturbative contributions from soft radiation. The state of the art for resummation in hadron collider event shapes is the next-to-leading logarithm (NLL) plus next-to-leading order (NLO) analysis in Ref. [4]. In this Letter we present results for the beam thrust cross section for $\tau_B \ll 1$ at next-to-next-to-leading-logarithmic (NNLL) order. This represents the first complete calculation to this order for a hadron collider event shape. Letting $v_B - i0$ be the Fourier conjugate variable to τ_B , the Fourier-transformed cross section exponentiates and has the form

$$\ln \frac{d\sigma}{dv_B} \sim L(\alpha_s L)^k + (\alpha_s L)^k + \alpha_s (\alpha_s L)^k + \dots, \quad (3)$$

where $L = \ln v_B$ and we sum over $k \geq 1$. Here, the three sets of terms are the leading logarithmic (LL), NLL, and NNLL corrections.

Beam Thrust Factorization Theorem. The Drell-Yan beam thrust cross section for small τ_B obeys the factorization theorem [6]

$$\begin{aligned} \frac{d\sigma}{dQ dY d\tau_B} &= \frac{8\pi\alpha_{\text{em}}^2}{9E_{\text{cm}}^2 Q} \sum_{ij} H_{ij}(Q^2, \mu_H) U_H(Q^2, \mu_H, \mu) \\ &\times \int dt_a dt'_a B_i(t_a - t'_a, x_a, \mu_B) U_B^i(t'_a, \mu_B, \mu) \\ &\times \int dt_b dt'_b B_j(t_b - t'_b, x_b, \mu_B) U_B^j(t'_b, \mu_B, \mu) \\ &\times \int dk Q S_B\left(\tau_B Q - \frac{t_a + t_b}{Q} - k, \mu_S\right) \\ &\times U_S(k, \mu_S, \mu), \end{aligned} \quad (4)$$

where $x_a = (Q/E_{\text{cm}})e^Y$ and $x_b = (Q/E_{\text{cm}})e^{-Y}$, E_{cm} is the total center-of-mass energy, and the sum runs over quark flavors $ij = \{u\bar{u}, \bar{u}u, d\bar{d}, \dots\}$. The hard function $H_{ij}(Q^2, \mu_H)$ contains virtual radiation at the hard scale Q (and also includes the leptonic process).

The beam functions $B_i(t_a, x_a, \mu_B)$ and $B_j(t_b, x_b, \mu_B)$ in Eq. (4) depend on the momentum fractions $x_{a,b}$ and virtualities $t_{a,b}$ of the partons i and j annihilated in the hard interaction. They can be calculated in an operator-product expansion [7, 8]

$$B_i(t_a, x_a, \mu_B) = \sum_k \int_{x_a}^1 \frac{d\xi_a}{\xi_a} \mathcal{I}_{ik}\left(t_a, \frac{x_a}{\xi_a}, \mu_B\right) f_k(\xi_a, \mu_B), \quad (5)$$

and analogously for B_j . Here, the sum runs over parton species $k = \{g, u, \bar{u}, d, \bar{d}, \dots\}$ and $f_k(\xi_a, \mu_B)$ denotes the standard parton distribution function (PDF) for parton k with momentum fraction ξ_a . The Wilson coefficients $\mathcal{I}_{ik}(t_a, z_a, \mu_B)$ describe the collinear virtual and real ISR emitted by this parton at the beam scale $\mu_B^2 \simeq t_a \simeq \tau_B Q^2$. The real ISR causes the formation of a jet prior to the hard collision which is observed as radiation centered around the beam axis. The PDFs in Eq. (5) are evaluated at the beam scale μ_B , because the measurement of τ_B introduces sensitivity to the virtualities $t \simeq \tau_B Q^2$ of the colliding hard partons, giving large logarithms $\ln(\mu_B^2/t)$.

For small τ_B , we have

$$\tau_B = \frac{t_a}{Q^2} + \frac{t_b}{Q^2} + \frac{k_B}{Q} + \mathcal{O}(\tau_B^2), \quad (6)$$

where the last term is the contribution from soft radiation at the scale $\mu_S \simeq k_B \simeq \tau_B Q$ and is described by the soft function $S_B(k_B, \mu_S)$ in Eq. (4). The collinear and soft contributions are not separately measurable, which leads to the convolution of S_B , B_i , and B_j in Eq. (4). $S_B(k_B, \mu_S)$ includes the effects of hadronization and soft radiation in the underlying event. For $\Lambda_{\text{QCD}} \ll \mu_S$, it is perturbatively calculable with power corrections of $\mathcal{O}(\Lambda_{\text{QCD}}/\mu_S)$.

The large logarithms $\alpha_s^n \ln^m \tau_B$, with $m \leq 2n$, are summed in Eq. (4) as follows. The hard, beam, and soft functions are each evaluated at their natural scale $|\mu_H| = Q$, $\mu_B = \sqrt{\tau_B} Q$, and $\mu_S = \tau_B Q$, respectively, where they contain no large logarithms and can be computed in fixed-order perturbation theory. They are then evolved to an arbitrary common scale μ by the evolution kernels U_H , $U_B^{i,j}$, and U_S , and this sums logarithms of the three scale ratios μ/μ_H , μ/μ_B , and μ/μ_S , respectively. The combination of the different evolution kernels in Eq. (4) is μ -independent and sums the logarithms of τ_B . The hard function for Drell-Yan production is a timelike form factor and for $\mu_H \simeq Q$ contains large π^2 terms from $\ln^2(-iQ/\mu_H)$. We sum these π^2 terms by taking $\mu_H = -iQ$ [9]. We estimate perturbative uncertainties by varying μ_H , μ_B , and μ_S about the above values. The complete summation at NNLL requires the NLO expressions for H_{ij} , \mathcal{I}_{qq} , \mathcal{I}_{qg} , and S_B , as well as the NNLL expressions for U_H , $U_B^{i,j}$, and U_S . See Ref. [8] for a discussion and references of the required anomalous dimensions and fixed-order computations.

Results at NNLL. In our numerical results we use the MSTW2008 NLO PDFs [10] with their $\alpha_s(m_Z) = 0.1208$. We also integrate over Y in Eq. (4). In Fig. 2, we show the Drell-Yan cross section $d\sigma/dQ$ with no cut at NLO and with cuts $\tau_B \leq \{0.1, 0.02\}$ at NNLL, for the LHC with $E_{\text{cm}} = 7$ TeV and for the Tevatron. The Z resonance is visible at $Q = m_Z$.

The cut $\tau_B \leq 0.1$ reduces the cross section only by a factor of around 1.3 above the Z peak (or 5–1.5 for $\tau_B \leq 0.02$), showing that most of the cross section comes

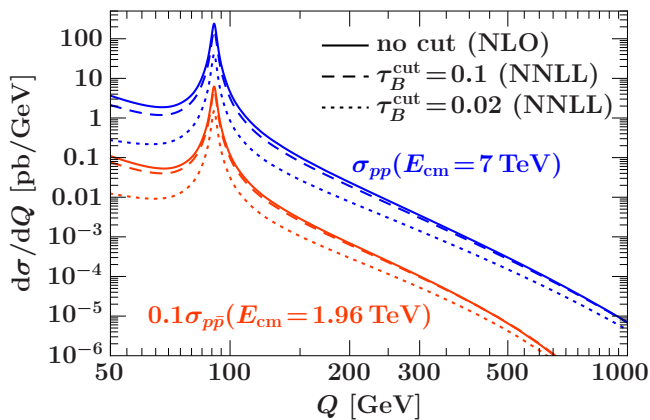


FIG. 2: Drell-Yan cross section $d\sigma/dQ$ with cuts $\tau_B \leq 0.1$ (dashed lines) and $\tau_B \leq 0.02$ (dotted lines) at NNLL. The solid lines show the total NLO cross section without a cut. For better distinction, the Tevatron cross section is multiplied by 0.1.

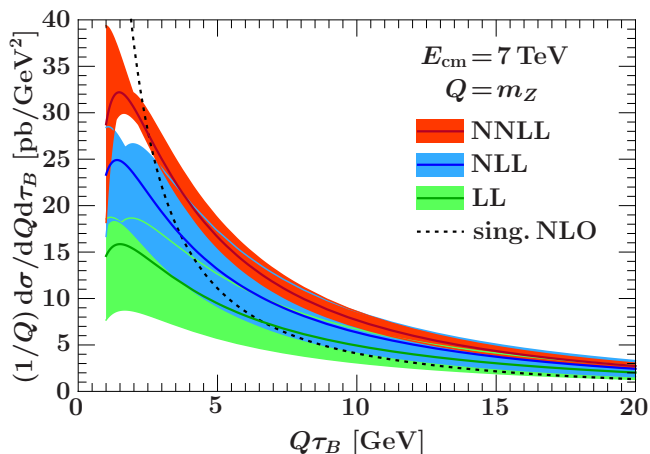


FIG. 3: Cross section differential in τ_B at $Q = m_Z$ for the LHC with $E_{\text{cm}} = 7$ TeV. Shown are the LL, NLL, and NNLL results, where the bands indicate the perturbative uncertainties as explained in the text. For comparison, the dotted line shows the singular NLO result with no resummation.

from small τ_B . The cross section differential in τ_B at fixed $Q = m_Z$ is shown in Fig. 3, where we can see explicitly that the cross section is dominated by small τ_B . To see the effect of the higher-order resummation we plot the LL, NLL, and NNLL results. The importance of resummation is illustrated by comparing them to the singular part of the fixed NLO result (dashed line), which is obtained from our NNLL result by setting $\mu_H = \mu_B = \mu_S = Q$. (The full NLO result contains additional nonsingular terms that are not numerically relevant at small τ_B .) Results are not plotted below $Q\tau_B = \mu_S \leq 1$ GeV, where the soft function becomes nonperturbative and we expect large corrections of $\mathcal{O}(\Lambda_{\text{QCD}}/\mu_S)$ to our purely perturbative results. Correspondingly, the perturbative uncertainties get large here.

In Fig. 4 we show the cross section integrated up to $\tau_B \leq \tau_B^{\text{cut}}$ as a function of $Q\tau_B^{\text{cut}}$ for $Q = m_Z$ and $Q = 300$ GeV. We see again that the logarithms are important at small τ_B^{cut} and need to be resummed.

In Figs. 3 and 4, the perturbative scale uncertainties are given by bands from varying μ_H , μ_B , and μ_S . The independent variation of these three scales would overestimate the uncertainty, since it does not take into account the parametric relation $\mu_B^2 \simeq \mu_S \mu_H$ and the hierarchy $\mu_S \ll \mu_B \ll \mu_H$. On the other hand, their simultaneous variation [case (a) in Eq. (7)] can produce unnaturally small scale uncertainties. Hence, the perturbative uncertainties in all figures are the envelope of the separate scale variations

$$\begin{aligned} \text{(a)} \quad & \mu_H = -riQ, \quad \mu_B = r\sqrt{\tau_B}Q, \quad \mu_S = r\tau_BQ, \\ \text{(b)} \quad & \mu_H = -iQ, \quad \mu_B = r^{-(\ln \tau_B)/4}\sqrt{\tau_B}Q, \quad \mu_S = \tau_BQ, \\ \text{(c)} \quad & \mu_H = -iQ, \quad \mu_B = \sqrt{\tau_B}Q, \quad \mu_S = r^{-(\ln \tau_B)/4}\tau_BQ, \end{aligned} \quad (7)$$

with $r = \{1/2, 2\}$, and $r = 1$ corresponding to the central-value curves. The exponent of r for cases (b) and (c) is chosen such that for $\tau_B = e^{-4}$ the scales μ_B or μ_S vary by factors of 2, with smaller variations for increasing τ_B and no variation for $\tau_B \rightarrow 1$. In this limit, there should only be a single scale $|\mu_H| = \mu_B = \mu_S$, and thus the only scale variation should be case (a). For the integrated cross section we replace τ_B in Eq. (7) with τ_B^{cut} . In both Figs. 3 and 4, we see good convergence of the perturbative series and a substantial reduction in the perturbative uncertainties at NNLL. The convergence is improved appreciably by the summation of the π^2 terms.

In Fig. 5, we plot percent differences for several cross sections relative to the NNLL result. All results are integrated up to $\tau_B^{\text{cut}} = 0.1$ and are plotted versus Q . The dark orange bands show the NNLL perturbative uncertainties and the light yellow bands the 90% C.L. PDF+ α_s uncertainties using the procedure from Ref. [10]. The dashed line shows the NNLL result without the gluon contribution to the quark beam function, \mathcal{I}_{qq} in Eq. (5). The gluon contribution is significant at the LHC and less prominent at the Tevatron, because the gluon PDF is more important for pp than $p\bar{p}$ collisions. In the dotted line we further neglect all terms in the quark contribution \mathcal{I}_{qq} that are subleading in the threshold limit $x \rightarrow 1$. Except for the Tevatron at large Q the threshold result is a poor approximation to the full result, being well outside the perturbative uncertainties. The dark band and solid line show the NLO result with the perturbative uncertainties from varying the common scale between $Q/2$ and $2Q$. Its difference from the resummed NNLL result is generically large and not captured by the fixed-order perturbative uncertainties, showing that the resummation is important not only to get an improved central value but also to obtain reliable perturbative uncertainties.

Beam thrust in Drell-Yan production provides an experimentally and theoretically clean measure of ISR in

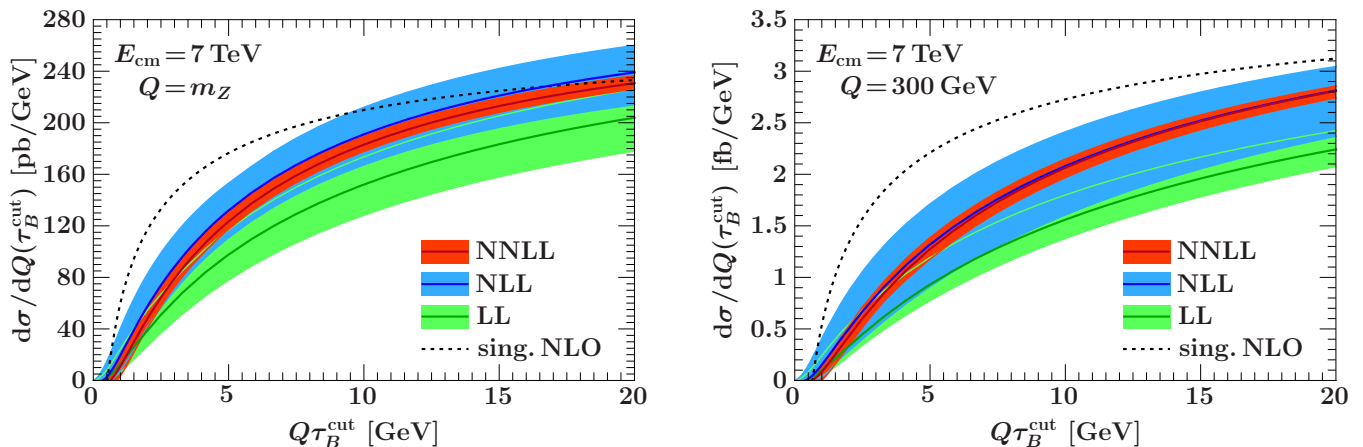


FIG. 4: Integrated cross section with a cut $\tau_B \leq \tau_B^{\text{cut}}$ as a function of τ_B^{cut} at $Q = m_Z$ (left panel) and $Q = 300$ GeV (right panel) for the LHC. The curves have the same meaning as in Fig. 3.

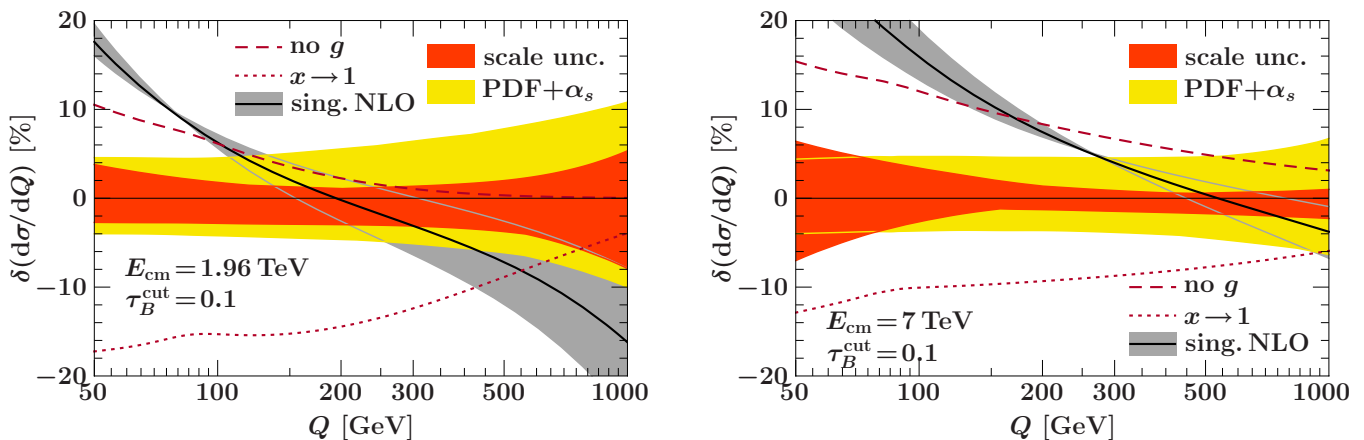


FIG. 5: Percent difference relative to the central NNLL result, $\delta(d\sigma/dQ) = (d\sigma/dQ)/(d\sigma^{\text{NNLL}}/dQ) - 1$, at the Tevatron (left panel) and the LHC (right panel). Here we always take $\tau_B^{\text{cut}} = 0.1$ in both the numerator and denominator.

$q\bar{q} \rightarrow \ell^+\ell^-$, similar to how thrust measures final-state radiation in $e^+e^- \rightarrow q\bar{q}$. The experimental measurement of beam thrust will contribute very valuable information to our understanding of ISR at hadron colliders and could be used to test and tune the initial-state parton shower and underlying event models in Monte Carlo programs. Restricting beam thrust $\tau_B \ll 1$ implements a theoretically well-controlled jet veto, which has important applications in other processes, for example, Higgs production [11]. The measurement of beam thrust in Drell-Yan provides a clean environment to test the application of beam thrust as a central jet veto.

This work was supported by the Office of Nuclear Physics of the U.S. Department of Energy, under Grant No. DE-FG02-94ER40818.

[1] S. Bethke, *Prog. Part. Nucl. Phys.* **58**, 351 (2007); S. Kluth, *Rept. Prog. Phys.* **69**, 1771 (2006).

[2] DELPHI Collaboration, P. Abreu *et al.*, *Z. Phys. C* **73**, 11 (1996); A. Buckley *et al.*, *Eur. Phys. J. C* **65**, 331 (2010).
 [3] Z. Nagy, *Phys. Rev. D* **68**, 094002 (2003).
 [4] A. Banfi, G. P. Salam, and G. Zanderighi, *JHEP* **08**, 062 (2004); *JHEP* **06**, 038 (2010).
 [5] G. Dissertori, F. Moortgat, and M. A. Weber, arXiv:0810.3208.
 [6] I. W. Stewart, F. J. Tackmann, and W. J. Waalewijn, *Phys. Rev. D* **81**, 094035 (2010); *Phys. Rev. Lett.* **105**, 092002 (2010).
 [7] S. Fleming, A. K. Leibovich, and T. Mehen, *Phys. Rev. D* **74**, 114004 (2006).
 [8] I. W. Stewart, F. J. Tackmann, and W. J. Waalewijn, *JHEP* **09**, 005 (2010).
 [9] L. Magnea and G. Sterman, *Phys. Rev. D* **42**, 4222 (1990); T. O. Eynck, E. Laenen, and L. Magnea, *JHEP* **06**, 057 (2003); V. Ahrens *et al.*, *Eur. Phys. J. C* **62**, 333 (2009).
 [10] A. D. Martin *et al.*, *Eur. Phys. J. C* **63**, 189 (2009); *Eur. Phys. J. C* **64**, 653 (2009).
 [11] C. F. Berger *et al.*, arXiv:1012.4480.